EUROPEAN ORGANIZATION FOR NUCLEAR RESEARCH

CERN–PPE/97–55

22 May 1997

Measurement of the Spin Density Matrix for the ρ^0, $K^{*0}(892)$ and ϕ Produced in Z^0 Decays

DELPHI Collaboration

Abstract

The spin density matrix elements for the ρ^0, $K^{*0}(892)$ and ϕ produced in hadronic Z^0 decays are measured in the DELPHI detector. There is no evidence for spin alignment of the $K^{*0}(892)$ and ϕ in the region $x_p \leq 0.3$ ($x_p = p/p_{beam}$), where $\rho_{00} = 0.33 \pm 0.05$ and $\rho_{00} = 0.30 \pm 0.04$, respectively. In the fragmentation region, $x_p \geq 0.4$, there is some indication for spin alignment of the ρ^0 and $K^{*0}(892)$, since $\rho_{00} = 0.43 \pm 0.05$ and $\rho_{00} = 0.46 \pm 0.08$, respectively. These values are compared with those found in meson-induced hadronic reactions. For the ϕ, $\rho_{00} = 0.30 \pm 0.04$ for $x_p \geq 0.4$ and 0.55 ± 0.10 for $x_p \geq 0.7$. The off-diagonal spin density matrix element ρ_{1-1} is consistent with zero in all cases.

(To be submitted to Physics Letters B)

P.Abreu[21], W.Adam[49], T.Adye[36], G.D.Alekseev[16], R.Alemany[48], P.P.Allport[22], S.Almehed[24], U.Amaldi[9], S.Amato[46], P.Andersson[43], A.Andreazza[9], P.Antilogus[9], W-D.Apel[17], Y.Arnoud[14], B.Åsman[43], J-E.Augustin[25], A.Augustinus[30], P.Baillon[9], P.Bambade[19], F.Barao[21], M.Barbi[46], G.Barbiellini[45], D.Y.Bardin[16], G.Barker[9], A.Baroncelli[39], O.Barring[24], M.J.Bates[36], M.Battaglia[15], M.Baubillier[23], J.Baudot[38], K-H.Becks[51], M.Begalli[6], P.Beilliere[8], Yu.Belokopytov[9,52], A.C.Benvenuti[5], C.Berat[14], M.Berggren[46], D.Bertini[25], D.Bertrand[2], M.Besancon[38], F.Bianchi[44], M.Bigi[44], M.S.Bilenky[16], P.Billoir[23], M-A.Bizouard[19], D.Bloch[10], M.Blume[51], M.Bonesini[27], W.Bonivento[27], P.S.L.Booth[22], A.W.Borgland[4], G.Borisov[38,41], C.Bosio[39], O.Botner[47], E.Boudinov[30], B.Bouquet[19], C.Bourdarios[19], T.J.V.Bowcock[22], M.Bozzo[13], P.Branchini[39], K.D.Brand[35], T.Brenke[51], R.A.Brenner[47], C.Bricman[2], R.C.A.Brown[9], P.Bruckman[18], J-M.Brunet[8], L.Bugge[32], T.Buran[32], T.Burgsmueller[51], P.Buschmann[51], S.Cabrera[48], M.Caccia[27], M.Calvi[27], A.J.Camacho Rozas[40], T.Camporesi[9], V.Canale[37], M.Canepa[13], F.Cao[2], F.Carena[9], L.Carroll[22], C.Caso[13], M.V.Castillo Gimenez[48], A.Cattai[9], F.R.Cavallo[5], V.Chabaud[9], M.Chapkin[41], Ph.Charpentier[9], L.Chaussard[25], P.Checchia[35], G.A.Chelkov[16], M.Chen[2], R.Chierici[44], P.Chliapnikov[41], P.Chochula[7], V.Chorowicz[25], J.Chudoba[29], V.Cindro[42], P.Collins[9], R.Contri[13], E.Cortina[48], G.Cosme[19], F.Cossutti[45], J-H.Cowell[22], H.B.Crawley[1], D.Crennell[36], G.Crosetti[13], J.Cuevas Maestro[33], S.Czellar[15], J.Dahm[51], B.Dalmagne[19], M.Dam[28], G.Damgaard[28], P.D.Dauncey[36], M.Davenport[9], W.Da Silva[23], A.Deghorain[2], G.Della Ricca[45], P.Delpierre[26], N.Demaria[34], A.De Angelis[9], W.De Boer[17], S.De Brabandere[2], C.De Clercq[2], C.De La Vaissiere[23], B.De Lotto[45], A.De Min[35], L.De Paula[46], H.Dijkstra[9], L.Di Ciaccio[37], A.Di Diodato[37], A.Djannati[8], J.Dolbeau[8], K.Doroba[50], M.Dracos[10], J.Drees[51], K.-A.Drees[51], M.Dris[31], J-D.Durand[25,9], D.Edsall[1], R.Ehret[17], G.Eigen[4], T.Ekelof[47], G.Ekspong[43], M.Elsing[9], J-P.Engel[10], B.Erzen[42], M.Espirito Santo[21], E.Falk[24], G.Fanourakis[11], D.Fassouliotis[45], M.Feindt[9], A.Fenyuk[41], P.Ferrari[27], A.Ferrer[48], S.Fichet[23], T.A.Filippas[31], A.Firestone[1], P.-A.Fischer[10], H.Foeth[9], E.Fokitis[31], F.Fontanelli[13], F.Formenti[9], B.Franek[36], A.G.Frodesen[4], R.Fruhwirth[49], F.Fulda-Quenzer[19], J.Fuster[48], A.Galloni[22], D.Gamba[44], M.Gandelman[46], C.Garcia[48], J.Garcia[40], C.Gaspar[9], U.Gasparini[35], Ph.Gavillet[9], E.N.Gazis[31], D.Gele[10], J-P.Gerber[10], L.Gerdyukov[41], R.Gokieli[50], B.Golob[42], P.Goncalves[21], G.Gopal[36], L.Gorn[1], M.Gorski[50], Yu.Gouz[44,52], V.Gracco[13], E.Graziani[39], C.Green[22], A.Grefrath[51], P.Gris[38], G.Grosdidier[19], K.Grzelak[50], M.Gunther[47], J.Guy[36], F.Hahn[9], S.Hahn[51], Z.Hajduk[18], A.Hallgren[47], K.Hamacher[51], F.J.Harris[34], V.Hedberg[24], R.Henriques[21], J.J.Hernandez[48], P.Herquet[2], H.Herr[9], T.L.Hessing[34], J.-M.Heuser[51], E.Higon[48], S-O.Holmgren[43], P.J.Holt[34], D.Holthuizen[30], S.Hoorelbeke[2], M.Houlden[22], J.Hrubec[49], K.Huet[2], K.Hultqvist[43], J.N.Jackson[22], R.Jacobsson[43], P.Jalocha[9], R.Janik[7], Ch.Jarlskog[24], G.Jarlskog[24], P.Jarry[38], B.Jean-Marie[19], E.K.Johansson[43], L.Jonsson[24], P.Jonsson[24], C.Joram[9], P.Juillot[10], M.Kaiser[17], F.Kapusta[23], K.Karafasoulis[11], S.Katsanevas[25], E.C.Katsoufis[31], R.Keranen[4], Yu.Khokhlov[41], B.A.Khomenko[16], N.N.Khovanski[16], B.King[22], N.J.Kjaer[30], O.Klapp[51], H.Klein[9], P.Kluit[30], D.Knoblauch[17], P.Kokkinias[11], M.Koratzinos[9], K.Korcyl[18], V.Kostioukhine[41], C.Kourkoumelis[3], O.Kouznetsov[13,16], M.Krammer[49], C.Kreuter[9], I.Kronkvist[24], J.Krstic[11], Z.Krumstein[16], W.Krupinski[18], P.Kubinec[7], W.Kucewicz[18], K.Kurvinen[15], C.Lacasta[9], I.Laktineh[25], J.W.Lamsa[1], L.Lanceri[45], D.W.Lane[1], P.Langefeld[51], J-P.Laugier[38], R.Lauhakangas[15], G.Leder[49], F.Ledroit[14], V.Lefebure[2], C.K.Legan[1], A.Leisos[11], R.Leitner[29], J.Lemonne[2], G.Lenzen[51], V.Lepeltier[19], T.Lesiak[18], J.Libby[34], D.Liko[9], A.Lipniacka[43], I.Lippi[35], B.Loerstad[24], J.G.Loken[34], J.M.Lopez[40], D.Loukas[11], P.Lutz[38], L.Lyons[34], J.MacNaughton[49], G.Maehlum[17], J.R.Mahon[6], A.Maio[21], T.G.M.Malmgren[43], V.Malychev[16], F.Mandl[49], J.Marco[40], R.Marco[40], B.Marechal[46], M.Margoni[35], J-C.Marin[9], C.Mariotti[9], A.Markou[11], C.Martinez-Rivero[33], F.Martinez-Vidal[48], S.Marti i Garcia[22], J.Masik[29], F.Matorras[40], C.Matteuzzi[27], G.Matthiae[37], M.Mazzucato[35], M.Mc Cubbin[22], R.Mc Kay[1], R.Mc Nulty[9], G.Mc Pherson[22], J.Medbo[47], C.Meroni[27], S.Meyer[17], W.T.Meyer[1], A.Miagkov[41], M.Michelotto[35], E.Migliore[44], L.Mirabito[25], W.A.Mitaroff[49], U.Mjoernmark[24], T.Moa[43], R.Moeller[28], K.Moenig[9], M.R.Monge[13], P.Morettini[13], H.Mueller[17], K.Muenich[51], M.Mulders[30], L.M.Mundim[6], W.J.Murray[36], B.Muryn[14,18], G.Myatt[34], T.Myklebust[32], F.Naraghi[14], F.L.Navarria[5], S.Navas[48], K.Nawrocki[50], P.Negri[27], S.Nemecek[12], W.Neumann[51], N.Neumeister[49], R.Nicolaidou[3], B.S.Nielsen[28], M.Nieuwenhuizen[30], V.Nikolaenko[10], M.Nikolenko[10,16], P.Niss[43], A.Nomerotski[35], A.Normand[22], A.Nygren[24], W.Oberschulte-Beckmann[17], V.Obraztsov[41], A.G.Olshevski[16], A.Onofre[21], R.Orava[15], G.Orazi[10], K.Osterberg[15], A.Ouraou[38], P.Paganini[19], M.Paganoni[9,27], R.Pain[23], H.Palka[18], Th.D.Papadopoulou[31], K.Papageorgiou[11], L.Pape[9], C.Parkes[34], F.Parodi[13], U.Parzefall[22], A.Passeri[39], M.Pegoraro[35], L.Peralta[21], H.Pernegger[49], M.Pernicka[49], A.Perrotta[5], C.Petridou[45], A.Petrolini[13], H.T.Phillips[36], G.Piana[13], F.Pierre[38], M.Pimenta[21], T.Podobnik[34], O.Podobrin[9], M.E.Pol[6], G.Polok[18], P.Poropat[45], V.Pozdniakov[16], P.Privitera[37], N.Pukhaeva[16], A.Pullia[27], D.Radojicic[34], S.Ragazzi[27], H.Rahmani[31], P.N.Ratoff[20], A.L.Read[32], M.Reale[51], P.Rebecchi[9], N.G.Redaelli[27], M.Regler[49], D.Reid[9], R.Reinhardt[51], P.B.Renton[34], L.K.Resvanis[3], F.Richard[19], J.Ridky[12], G.Rinaudo[44], O.Rohne[32], A.Romero[44], P.Ronchese[35], L.Roos[23], E.I.Rosenberg[1], P.Rosinsky[7], P.Roudeau[19], T.Rovelli[5], V.Ruhlmann-Kleider[38], A.Ruiz[40], K.Rybicki[18], H.Saarikko[15], Y.Sacquin[38], A.Sadovsky[16], G.Sajot[14], J.Salt[48], M.Sannino[13], H.Schneider[17], U.Schwickerath[17], M.A.E.Schyns[51], G.Sciolla[44], F.Scuri[45], P.Seager[20], Y.Sedykh[16], A.M.Segar[34], A.Seitz[17], R.Sekulin[36], L.Serbelloni[37], R.C.Shellard[6], A.Sheridan[22], P.Siegrist[9,38], R.Silvestre[38], F.Simonetto[35], A.N.Sisakian[16], T.B.Skaali[32], G.Smadja[25], N.Smirnov[41], O.Smirnova[24], G.R.Smith[36], A.Sokolov[41], O.Solovianov[41], R.Sosnowski[50], D.Souza-Santos[6], T.Spassov[21], E.Spiriti[39], P.Sponholz[51], S.Squarcia[13], D.Stampfer[9], C.Stanescu[39], S.Stanic[42], S.Stapnes[32], I.Stavitski[35], K.Stevenson[34], A.Stocchi[19], J.Strauss[49], R.Strub[10], B.Stugu[4], M.Szczekowski[50], M.Szeptycka[50], T.Tabarelli[27], J.P.Tavernet[23], F.Tegenfeldt[47], F.Terranova[27], J.Thomas[34], A.Tilquin[26], J.Timmermans[30], L.G.Tkatchev[16], T.Todorov[10], S.Todorova[10], D.Z.Toet[30], A.Tomaradze[2], A.Tonazzo[27], L.Tortora[39], G.Transtromer[24], D.Treille[9], G.Tristram[8], A.Trombini[19], C.Troncon[27], A.Tsirou[9], M-L.Turluer[38], I.A.Tyapkin[16], M.Tyndel[36], S.Tzamarias[11], B.Ueberschaer[51], O.Ullaland[9], V.Uvarov[41], G.Valenti[5], E.Vallazza[45], G.W.Van Apeldoorn[30], P.Van Dam[30], J.Van Eldik[30], A.Van Lysebetten[2], N.Vassilopoulos[34], G.Vegni[27], L.Ventura[35], W.Venus[36], F.Verbeure[2], M.Verlato[35], L.S.Vertogradov[16], D.Vilanova[38], P.Vincent[25], L.Vitale[45], E.Vlasov[41], A.S.Vodopyanov[16], V.Vrba[12], H.Wahlen[51], C.Walck[43], C.Weiser[17], A.M.Wetherell[9], D.Wicke[51], J.H.Wickens[2], M.Wielers[17], G.R.Wilkinson[9], W.S.C.Williams[34], M.Winter[10], M.Witek[18], T.Wlodek[19], J.Yi[1], K.Yip[34], O.Yushchenko[41], F.Zach[25], A.Zaitsev[41], A.Zalewska[9], P.Zalewski[50], D.Zavrtanik[42], E.Zevgolatakos[11], N.I.Zimin[16], G.C.Zucchelli[43], G.Zumerle[35]

[1] Department of Physics and Astronomy, Iowa State University, Ames IA 50011-3160, USA
[2] Physics Department, Univ. Instelling Antwerpen, Universiteitsplein 1, B-2610 Wilrijk, Belgium
and IIHE, ULB-VUB, Pleinlaan 2, B-1050 Brussels, Belgium
and Faculté des Sciences, Univ. de l'Etat Mons, Av. Maistriau 19, B-7000 Mons, Belgium
[3] Physics Laboratory, University of Athens, Solonos Str. 104, GR-10680 Athens, Greece
[4] Department of Physics, University of Bergen, Allégaten 55, N-5007 Bergen, Norway
[5] Dipartimento di Fisica, Università di Bologna and INFN, Via Irnerio 46, I-40126 Bologna, Italy
[6] Centro Brasileiro de Pesquisas Físicas, rua Xavier Sigaud 150, RJ-22290 Rio de Janeiro, Brazil
and Depto. de Física, Pont. Univ. Católica, C.P. 38071 RJ-22453 Rio de Janeiro, Brazil
and Inst. de Física, Univ. Estadual do Rio de Janeiro, rua São Francisco Xavier 524, Rio de Janeiro, Brazil
[7] Comenius University, Faculty of Mathematics and Physics, Mlynska Dolina, SK-84215 Bratislava, Slovakia
[8] Collège de France, Lab. de Physique Corpusculaire, IN2P3-CNRS, F-75231 Paris Cedex 05, France
[9] CERN, CH-1211 Geneva 23, Switzerland
[10] Institut de Recherches Subatomiques, IN2P3 - CNRS/ULP - BP20, F-67037 Strasbourg Cedex, France
[11] Institute of Nuclear Physics, N.C.S.R. Demokritos, P.O. Box 60228, GR-15310 Athens, Greece
[12] FZU, Inst. of Physics of the C.A.S. High Energy Physics Division, Na Slovance 2, 180 40, Praha 8, Czech Republic
[13] Dipartimento di Fisica, Università di Genova and INFN, Via Dodecaneso 33, I-16146 Genova, Italy
[14] Institut des Sciences Nucléaires, IN2P3-CNRS, Université de Grenoble 1, F-38026 Grenoble Cedex, France
[15] Helsinki Institute of Physics, HIP, P.O. Box 9, FIN-00014 Helsinki, Finland
[16] Joint Institute for Nuclear Research, Dubna, Head Post Office, P.O. Box 79, 101 000 Moscow, Russian Federation
[17] Institut für Experimentelle Kernphysik, Universität Karlsruhe, Postfach 6980, D-76128 Karlsruhe, Germany
[18] Institute of Nuclear Physics and University of Mining and Metalurgy, Ul. Kawiory 26a, PL-30055 Krakow, Poland
[19] Université de Paris-Sud, Lab. de l'Accélérateur Linéaire, IN2P3-CNRS, Bât. 200, F-91405 Orsay Cedex, France
[20] School of Physics and Chemistry, University of Lancaster, Lancaster LA1 4YB, UK
[21] LIP, IST, FCUL - Av. Elias Garcia, 14-1^o, P-1000 Lisboa Codex, Portugal
[22] Department of Physics, University of Liverpool, P.O. Box 147, Liverpool L69 3BX, UK
[23] LPNHE, IN2P3-CNRS, Universités Paris VI et VII, Tour 33 (RdC), 4 place Jussieu, F-75252 Paris Cedex 05, France
[24] Department of Physics, University of Lund, Sölvegatan 14, S-22363 Lund, Sweden
[25] Université Claude Bernard de Lyon, IPNL, IN2P3-CNRS, F-69622 Villeurbanne Cedex, France
[26] Univ. d'Aix - Marseille II - CPP, IN2P3-CNRS, F-13288 Marseille Cedex 09, France
[27] Dipartimento di Fisica, Università di Milano and INFN, Via Celoria 16, I-20133 Milan, Italy
[28] Niels Bohr Institute, Blegdamsvej 17, DK-2100 Copenhagen 0, Denmark
[29] NC, Nuclear Centre of MFF, Charles University, Areal MFF, V Holesovickach 2, 180 00, Praha 8, Czech Republic
[30] NIKHEF, Postbus 41882, NL-1009 DB Amsterdam, The Netherlands
[31] National Technical University, Physics Department, Zografou Campus, GR-15773 Athens, Greece
[32] Physics Department, University of Oslo, Blindern, N-1000 Oslo 3, Norway
[33] Dpto. Fisica, Univ. Oviedo, Avda. Calvo Sotelo, S/N-33007 Oviedo, Spain, (CICYT-AEN96-1681)
[34] Department of Physics, University of Oxford, Keble Road, Oxford OX1 3RH, UK
[35] Dipartimento di Fisica, Università di Padova and INFN, Via Marzolo 8, I-35131 Padua, Italy
[36] Rutherford Appleton Laboratory, Chilton, Didcot OX11 OQX, UK
[37] Dipartimento di Fisica, Università di Roma II and INFN, Tor Vergata, I-00173 Rome, Italy
[38] CEA, DAPNIA/Service de Physique des Particules, CE-Saclay, F-91191 Gif-sur-Yvette Cedex, France
[39] Istituto Superiore di Sanità, Ist. Naz. di Fisica Nucl. (INFN), Viale Regina Elena 299, I-00161 Rome, Italy
[40] Instituto de Fisica de Cantabria (CSIC-UC), Avda. los Castros, S/N-39006 Santander, Spain, (CICYT-AEN96-1681)
[41] Inst. for High Energy Physics, Serpukov P.O. Box 35, Protvino, (Moscow Region), Russian Federation
[42] J. Stefan Institute, Jamova 39, SI-1000 Ljubljana, Slovenia and Department of Astroparticle Physics, School of Environmental Sciences, Kostanjeviska 16a, Nova Gorica, SI-5000 Slovenia,
and Department of Physics, University of Ljubljana, SI-1000 Ljubljana, Slovenia
[43] Fysikum, Stockholm University, Box 6730, S-113 85 Stockholm, Sweden
[44] Dipartimento di Fisica Sperimentale, Università di Torino and INFN, Via P. Giuria 1, I-10125 Turin, Italy
[45] Dipartimento di Fisica, Università di Trieste and INFN, Via A. Valerio 2, I-34127 Trieste, Italy
and Istituto di Fisica, Università di Udine, I-33100 Udine, Italy
[46] Univ. Federal do Rio de Janeiro, C.P. 68528 Cidade Univ., Ilha do Fundão BR-21945-970 Rio de Janeiro, Brazil
[47] Department of Radiation Sciences, University of Uppsala, P.O. Box 535, S-751 21 Uppsala, Sweden
[48] IFIC, Valencia-CSIC, and D.F.A.M.N., U. de Valencia, Avda. Dr. Moliner 50, E-46100 Burjassot (Valencia), Spain
[49] Institut für Hochenergiephysik, Österr. Akad. d. Wissensch., Nikolsdorfergasse 18, A-1050 Vienna, Austria
[50] Inst. Nuclear Studies and University of Warsaw, Ul. Hoza 69, PL-00681 Warsaw, Poland
[51] Fachbereich Physik, University of Wuppertal, Postfach 100 127, D-42097 Wuppertal, Germany
[52] On leave of absence from IHEP Serpukhov

1 Introduction

With the large statistics presently accumulated by the LEP experiments, the inclusive production characteristics of at least one state per isospin multiplet have been measured for the SU(3) pseudoscalar and vector meson nonets, and for the baryon octet and decuplet. This has allowed tuning of a number of adjustable parameters in the QCD-based Monte Carlo models to get a reasonable description of the experimental data, thus obtaining useful information about the nature of the fragmentation process (see [1] and references therein).

The study of the spin properties of hadrons produced in e^+e^- annihilation is much less advanced. In the present versions of the commonly used Monte Carlo programs based on the Lund string model [2] and QCD cluster model [3], the particle spins enter only through adjustable phenomenological parameters accounting for the vector-pseudoscalar and decuplet-octet ratios. Otherwise the hadrons are treated as spinless objects. However, measurements of spin observables in quark fragmentation in e^+e^- reactions might be of interest. In particular, more can be learnt about the hadronization process from the alignment of the vector meson spins.

The spin alignment can be described in terms of the spin density matrix $\rho_{\lambda,\lambda'}$, which is a 3 x 3 Hermitian matrix with unit trace usually defined in the helicity basis.

Its diagonal elements, ρ_{11}, ρ_{-1-1}, and ρ_{00}, represent the relative intensities of the helicity $\lambda = +1$, $\lambda = -1$ and $\lambda = 0$ states. Since vector mesons decay strongly, there are no interference effects like those in parity non-conserving weak decays and the values of ρ_{11} and ρ_{-1-1} can not be measured separately. Therefore only one diagonal element ρ_{00} is measurable. A state of no spin alignment corresponds to $\rho_{00} = 1/3$. For inclusively produced vector mesons in e^+e^- annihilation, the values of ρ_{00} in the helicity frame predicted by different models [4–9] span the range $0 \leq \rho_{00} \leq 1$, depending on the assumptions made about the fragmentation process.

The off-diagonal elements of the spin density matrix measure the correlations between states with different helicities. In general, in the meson helicity rest frame considered in this paper, these elements are expected to be small. However, according to some theoretical expectations [10–12], coherence phenomena due to final-state interactions between the primary quark and antiquark may result in non-zero values of $\mathrm{Re}\rho_{1-1}$ and $\mathrm{Im}\rho_{1-1}$ for the vector mesons.

The spin density matrix elements have been measured previously for $D^{*\pm}$ mesons produced inclusively in e^+e^- collisions at energies up to $\sqrt{s} = 29$ GeV [13–15]. No strong evidence for spin alignment was found. More recently, they have been measured at LEP for the B^* [16–18], and for the $D^{*\pm}$ and ϕ [18]. For the B^*, the results of all three experiments [16–18] are consistent with no spin alignment. However, for the high energy ϕ, and perhaps for the $D^{*\pm}$, evidence for preferential production in the helicity zero state is observed [18].

This paper describes measurements of the spin density matrix elements for the ρ^0, $K^{*0}(892)$ and ϕ vector mesons† produced in Z^0 hadronic decays at LEP. The DELPHI results on the inclusive production properties of these mesons can be found elsewhere [19,20].

†Unless otherwise stated, antiparticles are implicitly included.

2 Experimental Procedure

The data collected by the DELPHI experiment in 1994, when the DELPHI Ring Imaging Cherenkov (RICH) detectors were fully operational and providing good particle identification, were used for the measurement of the spin density matrix for the $K^{*0}(892)$ in all x_p regions ($x_p = p/p_{beam}$), and for the ϕ in the region $0.05 \leq x_p \leq 0.3$. The sample corresponds to a total of 1.34 million hadronic Z^0 decays.

The spin density matrix for the ρ^0 and ϕ in the fragmentation region $x_p > 0.3$ was measured using the data sample with 3.3 million hadronic events collected by DELPHI in 1992-1995, without use of particle identification.

2.1 Event and particle selection

Detailed descriptions of the DELPHI detector and its performance can be found elsewhere [21,22].

The charged particle tracks were measured in the 1.2 T magnetic field by a set of tracking detectors. The average momentum resolution for charged particles in hadronic final states was usually between $\Delta p/p \simeq 0.001p$ and $0.01p$ (p in GeV/c), depending on which detectors were included in the track fit.

A charged particle was accepted in this analysis if its momentum p was greater than 0.2 GeV/c, its momentum error Δp was less than p, its polar angle with respect to the beam axis was between 25° and 155°, its measured track length in the Time Projection Chamber (TPC) was greater than 50 cm, and its impact parameter with respect to the nominal crossing point was within 5 cm in the transverse (xy) plane and 10 cm along the beam direction (z-axis).

Hadronic events were then selected by requiring at least 5 charged particles, a total energy of charged particles (assumed to be pions) above 3 GeV in each of the two hemispheres defined with respect to the beam direction, a total energy of all charged particles above 15 GeV, and a polar angle of the sphericity axis between 40° and 140°. For the analyses in which particle identification was used, information from the RICH detectors had to be available for at least one charged particle.

The samples selected with the above cuts comprised 0.85 and 2.12 million events collected in 1994 and in 1992-1995, respectively. The contamination from events due to beam-gas scattering and to $\gamma\gamma$ interactions was estimated to be less than 0.1%, and the background from $\tau^+\tau^-$ events less than 0.2% of the accepted events.

After the event selection, in order to ensure a better signal-to-background ratio for the resonances in the $\pi^+\pi^-$, $K^\pm\pi^\mp$, and K^+K^- invariant mass spectra, stronger restrictions were imposed on the track impact parameters with respect to the nominal crossing point: they had to be within 0.3 cm in the transverse plane and 2 cm along the beam direction.

Charged kaon identification was provided by the RICH detectors, as in the previous DELPHI analysis of inclusive production of the $K^{*0}(892)$ and ϕ [20]. The identification performance was evaluated by means of the detector simulation program DELSIM [22]. In DELSIM, about 4.9 million events satisfying the same selection criteria as the real data were generated using the JETSET program [23] with the DELPHI default parameters [24]. The particles were followed through the detector, and the simulated digitizations obtained were processed with the same reconstruction programs as the experimental data. The efficiency of kaon identification was found to be about 70% on average.

Kaon identification was required for the $K^\pm\pi^\mp$ mass distributions. For the K^+K^-mass spectra, at least one particle had to be identified as a kaon in the region $x_p \leq 0.3$, while all charged particles were assigned the kaon mass in the region $x_p > 0.3$. The $\pi^+\pi^-$ mass distributions were analysed without using particle identification, assuming all charged particles to be pions.

2.2 Fit procedure and treatment of detector imperfections

Particle identification inefficiencies as well as other detector imperfections, such as limited geometrical acceptance, particle interactions in the detector material, and the different kinematical cuts imposed for charged particle and event selection, were taken into account by applying the approach described in refs. [19,20,25] and outlined here.

In the present analysis a vector $\vec{a}$ of parameters was used in the definition of the anticipated distribution function, $f(M, \vec{a})$, of the invariant mass M. The parameters $\vec{a}$ were then determined by a least squares fit of the function to the data.

The function $f(M, \vec{a})$ was composed of three parts:

$$f(M, \vec{a}) = f^S(M, \vec{a}) + f^B(M, \vec{a}) + f^R(M, \vec{a}), \tag{1}$$

corresponding to the signal, background, and reflection contributions, respectively.

The signal function, $f^S(M, \vec{a})$, described the resonance signals in the corresponding invariant mass distributions. For the $\pi^+\pi^-$ mass distributions, it had a form:

$$\begin{aligned} f^S(M, \vec{a}) = a_1 PS_{\rho^0}(M) \cdot BW_{\rho^0}(M, a_2, a_3) \ &+ a_4 PS_{f_0}(M) \cdot BW_{f_0}(M, a_5, a_6) \\ &+ a_7 PS_{f_2}(M) \cdot BW_{f_2}(M, a_8, a_9) \end{aligned} \tag{2}$$

with the relativistic Breit–Wigner functions BW for the ρ^0, $f_0(980)$ and $f_2(1270)$ multiplied by the functions $PS(M)$ accounting for distortion of the resonance Breit–Wigner shapes by phase space effects (see [19] for details). For the $\mathrm{K}^\pm\pi^\mp$ mass distributions only two Breit–Wigner terms, representing the $\mathrm{K}^{*0}(892)$ and $\mathrm{K}_2^{*0}(1430)$, contributed to $f^S(M, \vec{a})$. For the $\mathrm{K}^+\mathrm{K}^-$ mass distribution only the ϕ was considered.

The background term, $f^B(M, \vec{a})$, was taken to be of the form

$$f^B(M, \vec{a}) = a_{10}(M - M_{th})^{a_{11}} \cdot \exp(a_{12}M + a_{13}M^2 + a_{14}M^3) \tag{3}$$

for the $\pi^+\pi^-$ mass distributions, where M_{th} is the invariant mass threshold. The same form was used for the background parametrization for the $\mathrm{K}^\pm\pi^\mp$ mass distribution. For the $\mathrm{K}^+\mathrm{K}^-$ mass spectra only the linear term in the exponential in Eq. 3 was used.

The third term, $f^R(M, \vec{a})$, represented the sum of all the reflection functions (RF_i):

$$f^R(M, \vec{a}) = \sum_i a_i RF_i(M). \tag{4}$$

Two types of reflection functions contributing to Eq. 4 were considered, as was discussed in detail in [19,20]. Reflections of the first type arise from imperfect particle identification (when, for example, resonances in the $\pi^+\pi^-$ and $\mathrm{K}^+\mathrm{K}^-$ systems distort the $\mathrm{K}^\pm\pi^\mp$ mass spectra). Those of the second type arise from resonance and particle decays in the same system, for example from $\mathrm{K}_S^0 \to \pi^+\pi^-$ or $\omega \to \pi^+\pi^- X$ in the $\pi^+\pi^-$ mass spectra, or from charmed particle production.

Although all possible reflections were considered, only the most important ones were finally taken into account. The ones considered were a) from the η, η', ω, ϕ, K_S^0, $\mathrm{K}^{*0}(892)$, $\mathrm{K}_2^{*0}(1430)$, $f_2'(1525)$ and D^0 in the $\pi^+\pi^-$ mass spectra, b) from the η, ω, ρ^0, ϕ, $f_0(980)$, $f_2(1270)$, $f_2'(1525)$, D^0, D^+ and D^{*+} in the $\mathrm{K}^\pm\pi^\mp$ mass spectra, and c) from the η, η', ω, ρ^0, $f_0(980)$, K_S^0, $\mathrm{K}^{*0}(892)$, D^0, D^+, D^{*+} and D_S^+ in the $\mathrm{K}^+\mathrm{K}^-$ mass spectra.

All reflections were found to be important for the $\pi^+\pi^-$ mass spectra, treated without particle identification. The $K^{*0}(892)$ signal in the $K^\pm\pi^\mp$ mass spectra was mostly affected by reflections from the ϕ for values of the helicity decay angle $\cos\theta_h$ (defined in section 3) near -1, and from the D^{*+} for $\cos\theta_h$ near $+1$. The influence of reflections on the ϕ signal selection was found to be very small.

The functions $RF_i(M)$ in Eq. 4 were determined from events generated according to the JETSET model. The contributions of the reflections to the uncorrected mass spectra defined by the function $\bar{N}^R_m(\vec{a})$ (see Eq. 6 below) were then obtained by passing these events through the detector simulation. This also accounted properly for the influence of particle misidentification.

In each mass bin, m, the number of entries $\bar{N}_m(\vec{a})$ predicted by the function $f(M,\vec{a})$ is given by:

$$\bar{N}_m(\vec{a}) = \bar{N}^S_m(\vec{a}) + \bar{N}^B_m(\vec{a}) + \bar{N}^R_m(\vec{a}), \tag{5}$$

where

$$\bar{N}^G_m(\vec{a}) = C^G_m \sum_n S^G_{mn} A^G_n f^G_n(\vec{a}), \tag{6}$$

$$f^G_n(\vec{a}) = \int_{M_n}^{M_{n+1}} f^G(M,\vec{a})dM, \tag{7}$$

where $G = S, B$, or R, and M_n is the lower edge of the n-th histogram bin in the distribution of the variable M. The coefficients A_n characterize the detector acceptance and the losses of particles due to the selection criteria imposed, and the C_m take into account the extra particles due to ghosts, secondary interactions, etc. The smearing matrix S_{mn} is determined by the experimental resolution. The three terms in Eq. 5 are all necessary (see [20,25] for more details) because the resonance signals, for example in the $K^\pm\pi^\mp$ invariant mass distribution, contain by definition only the $K^\pm\pi^\mp$ pairs, while the background is contaminated by the misidentified $\pi^+\pi^-$, K^+K^-, $K^\pm p^\mp$ and $p^\pm\pi^\mp$ pairs. Therefore the coefficients A_n and C_m for the resonance signals and for the background are expected to be different.

The A_n, C_m, and S_{mn} were estimated using the detector simulation program DELSIM (see [19] for more details). Due to differences in the detector performance and data processing in different running periods, the events generated by DELSIM for these periods were taken with relative weights corresponding to the relative numbers of corresponding events in the real data. By including the loss of particles due to the selection criteria in the coefficients A_n (instead of in C_m as was done in [19,20,25]), the coefficients C_m for the resonance signals became practically independent of the mass M.

The treatment of residual Bose-Einstein correlations affecting the Breit-Wigner shape of the resonances was also different from the procedure used in refs. [19,20,25]. The distortion of the resonance mass by this effect was accounted for by calculating, in each event generated by JETSET with the DELPHI default parameters [24], the resonance masses M_n and M_l before and after switching on the Bose-Einstein effect, and thus constructing the corresponding matrix $S^S_{ln}(BE)$, satisfying the normalization conditions $\sum_l S^S_{ln}(BE) = 1$. The final matrix S^S_{mn} for the resonances in Eq. 6 is the product of the usual smearing matrix accounting for the experimental resolution $S^S_{ml}(resol.)$ and the matrix $S^S_{ln}(BE)$ accounting for Bose-Einstein effects:

$$S^S_{mn} = \sum_l S^S_{ml}(resol.) S^S_{ln}(BE). \tag{8}$$

The Bose-Einstein effect was found to be important for the ρ^0 [19], very small for the $K^{*0}(892)$ [20] and was neglected for the ϕ.

The best values for $\vec{a}$ were then determined by a least squares fit of the predictions of Eq. 5 to the measured values, N_m, by minimizing the function:

$$\chi^2 = \sum_m (N_m - \bar{N}_m(\vec{a}))^2/\sigma_m^2 + \sum_i (a_i - \bar{a}_i)^2/(\Delta\bar{a}_i)^2, \tag{9}$$

where $\sigma_m^2 = N_m + \sigma^2(\bar{N}_m)$ and $\sigma(\bar{N}_m)$ is the error of $\bar{N}_m$ due to the finite statistics of the simulation used to evaluate A_n, C_m and S_{mn}. The second sum in Eq. 9 constrains some of the fitted parameters a_i to the values $\bar{a}_i \pm \Delta\bar{a}_i$ taken from external sources. In particular, the normalization of the reflection functions to the particle production rates taken from other experiments, and the masses and widths taken from the PDG tables [26], were used as constraints in this second term. Thus the "statistical" errors obtained from the fits include the corresponding systematic components.

The fits were made in the mass ranges from 0.3 to 1.8 GeV/c^2 for the $\pi^+\pi^-$, from 0.64 to 1.3 GeV/c^2 for the $\mathrm{K}^\pm\pi^\mp$, and from 0.988 to 1.1 GeV/c^2 or from 0.988 to 1.06 GeV/c^2 for the $\mathrm{K}^+\mathrm{K}^-$ mass spectra.

The resonance production rates were calculated as

$$\langle N \rangle = \frac{1}{Br}\frac{1}{\langle R \rangle}\int f^S(M,\vec{a})\, dM, \tag{10}$$

where the factor $1/Br$ takes into account the unobserved decay modes, and the integration limits are the same as the fit ranges. The factor $\langle R \rangle$, practically independent of the mass M, takes account of the imperfection of the detector simulation when the stronger cuts on impact parameters are applied. It was very close to the unity for the reprocessed 1994 data, but not for the rest of the data (see [19,20] for more details).

3 Results and Discussion

The spin density matrix was determined in the meson helicity rest frame with the quantization z-axis along the meson direction in the laboratory frame. The y-axis was defined as the vector product of the direction of the vector meson and the e^- beam direction. The azimuthal angle, φ, is equal to zero in the production plane defined by the vector meson momentum and the e^- beam direction. The polar angle, θ_h, is the helicity angle of the resonance, i.e. the angle of the π^+ from the ρ^0, the $\mathrm{K}^\pm$ from the $\mathrm{K}^{*0}(892)$, and the K^+ from the ϕ with respect to the z-axis in the resonance rest frame.

For $J^P = 1^-$ states, the distributions in $\cos\theta_h$ and φ may be written as

$$W(\cos\theta_h) = \frac{3}{4}(1-\rho_{00}) + \frac{3}{4}(3\rho_{00}-1)\cos^2\theta_h, \tag{11}$$

$$W(\varphi) = \frac{1}{2\pi}(1 + 2\mathrm{Im}\rho_{1-1}\sin 2\varphi - 2\mathrm{Re}\rho_{1-1}\cos 2\varphi). \tag{12}$$

The distributions in φ were folded in such way that $\varphi \to \varphi + \pi$ for $\varphi < 0$. For the ρ^0 and ϕ, with the same decay particles, the distributions in $\cos\theta_h$ were folded around $\cos\theta_h = 0$. For the $\mathrm{K}^{*0}(892)$, the full range $-1 \le \cos\theta_h \le 1$ was used, except for $0.1 \le x_p \le 0.3$ where only the range $\cos\theta_h \le 0$ was used (for the reasons discussed in [20]).

3.1 Spin Density Matrix

The spin density matrix for the $\mathrm{K}^{*0}(892)$ and ϕ was first analysed in the region of relatively small x_p. The corresponding analysis for the ρ^0 in this region was not possible due to the small signal to background ratio.

The measured uncorrected $K^{\pm}\pi^{\mp}$ invariant mass distributions for $0.1 \leq x_p \leq 0.3$ and for three $\cos\theta_h$ intervals are presented in Fig. 1a-c. The K^+K^- mass spectra for $0.05 \leq x_p \leq 0.3$ and for three $|\cos\theta_h|$ intervals are shown in Fig. 1d-f. In both cases, at least one kaon was required to be identified by the RICH. The $K^{*0}(892)$ and ϕ signals are clearly seen, and the fits describe the data quite well in all $\cos\theta_h$ intervals: the values of χ^2/NDF are equal to 21/27, 15/27, and 34/27 for Figs. 1a-c, and 58/52, 81/52, and 81/52 for Figs. 1d-f[‡]. The first four values indicate excellent fits; the last two acceptable fits. Notice that the structure at about 0.8 GeV/c^2 in Fig. 1a is explained by reflection from the ϕ, which is most important for $\cos\theta_h \to -1$; it is also well reproduced by the fit.

The $\cos\theta_h$ distributions for the $K^{*0}(892)$ and ϕ were obtained by determining the resonance cross-sections for different $\cos\theta_h$ intervals from fits to the corresponding invariant mass distributions shown in Fig. 1. They are presented in Fig. 2. The fit of these $\cos\theta_h$ distributions to the function (11) (shown by the curves in Fig. 2), and of the φ distributions to the function (12) (not shown), gave the values of the spin density matrix elements presented in the upper part of Table 1.

Table 1: Spin density matrix elements ρ_{00}, Reρ_{1-1}, Imρ_{1-1} for the ρ^0, $K^{*0}(892)$ and ϕ for different x_p ranges. The statistical and systematic errors are combined quadratically.

Particle	x_p range	ρ_{00}	Reρ_{1-1}	Imρ_{1-1}
$K^{*0}(892)$	$0.1 \leq x_p \leq 0.3$	0.33±0.05	0.00±0.02	-0.01±0.02
ϕ	$0.05 \leq x_p \leq 0.3$	0.30±0.04	0.00±0.02	0.00±0.02
ρ^0		0.42±0.04	0.00±0.02	0.00±0.02
$K^{*0}(892)$	$x_p \geq 0.3$	0.41±0.07	0.01±0.03	-0.01±0.03
ϕ		0.27±0.04	0.00±0.02	0.00±0.02
ρ^0		0.43±0.05	0.01±0.02	-0.01±0.02
$K^{*0}(892)$	$x_p \geq 0.4$	0.46±0.08	0.00±0.03	-0.03±0.03
ϕ		0.30±0.04	0.01±0.02	-0.01±0.02
ρ^0		0.48±0.06	0.02±0.03	0.00±0.03
$K^{*0}(892)$	$x_p \geq 0.5$	0.47±0.10	-0.02±0.04	-0.06±0.04
ϕ		0.36±0.06	0.02±0.03	0.00±0.03
ϕ	$x_p \geq 0.7$	0.55±0.10	0.02±0.04	0.00±0.04

The values

$$\rho_{00}(K^{*0}(892)) = 0.33 \pm 0.05 \tag{13}$$

and

$$\rho_{00}(\phi) = 0.30 \pm 0.04 \tag{14}$$

obtained for the $K^{*0}(892)$ and ϕ in the region of small x_p are close to the value of 1/3 expected for no spin alignment. This is quite understandable, since many of the light meson resonances in the small x_p region come from the decays of heavier objects.

In the next step, the spin density matrices for the ρ^0, $K^{*0}(892)$ and ϕ were measured in the fragmentation regions $x_p \geq 0.3$, $x_p \geq 0.4$, $x_p \geq 0.5$ and also in the region $x_p \geq 0.7$

[‡]For the other fits to be presented in the paper, the values of χ^2/NDF also indicate acceptable fits.

for the ϕ alone. The measured uncorrected $\pi^+\pi^-$, $K^\pm\pi^\mp$, and K^+K^- invariant mass distributions for $x_p \geq 0.4$ and for different $\cos\theta_h$ and φ intervals are shown in Figs. 3 - 5.

For the $\pi^+\pi^-$ mass spectra, the signal to background ratios for the ρ^0 are rather small (Fig. 3), but the high statistics allow the ρ^0 cross-sections to be determined in different $|\cos\theta_h|$ and φ intervals with good statistical precision. The fits describe the data well; note the presence of $f_0(980)$ signals on the right-hand-side shoulder of the ρ^0 peak. The signal to background ratios are larger for the narrower $K^{*0}(892)$ (see Fig. 4), and especially for the ϕ (see Fig. 5). Here again the fits provide a good description of the data. Large distortions of the $K^\pm\pi^\mp$ mass distributions by the reflections from the ϕ (Fig. 4a) and from the D^{*+} (Fig. 4f) on the left-hand-side of the $K^{*0}(892)$ are also well described by the fits.

The $\cos\theta_h$ and φ distributions for the ρ^0, $K^{*0}(892)$ and ϕ determined from the fits of the invariant mass distributions shown in Figs. 3-5 are presented in Fig. 6. The fit of the $\cos\theta_h$ distributions to the function (11) (see the curves in Fig. 6a, c, e) gave the values of the spin density matrix element for $x_p \geq 0.4$

$$\rho_{00}(\rho^0) = 0.43 \pm 0.05, \tag{15}$$

$$\rho_{00}(K^{*0}(892)) = 0.46 \pm 0.08, \tag{16}$$

$$\rho_{00}(\phi) = 0.30 \pm 0.04. \tag{17}$$

All values for different x_p ranges are collected in Table 1. It also shows the values of the off-diagonal matrix elements $\mathrm{Re}\rho_{1-1}$ and $\mathrm{Im}\rho_{1-1}$ for these mesons obtained from the fit of the φ distributions to the function (12) (see Fig. 6b, d, f) for $x_p \geq 0.4$).

In the high x_p region, the $K^{*0}(892)$ and ρ^0 appear to be produced with unequal population of the three helicity states with an indication that the helicity zero state is preferentially occupied. For the ϕ in the same x_p region, no spin alignment is observed. Some difference between the spin alignment of the ϕ and ρ^0 and $K^{*0}(892)$ might be perhaps related to mixing of the ϕ and ω. Anyhow, the preference for the helicity zero state appears to occur at still higher x_p values for the ϕ than for the ρ^0 and $K^{*0}(892)$. Indeed for the ϕ in the region $x_p \geq 0.7$, $\rho_{00} = 0.55 \pm 0.10$, in agreement with the value of $\rho_{00} = 0.54 \pm 0.08$ recently measured in the same $x_p \geq 0.7$ range by OPAL [18].

3.2 Systematic Errors

In Table 1, the statistical and systematic errors are combined quadratically. The systematic errors were first estimated in the same way as in [19,20] by determining the contributions arising from:

1. variations of the charged particle selection cuts;
2. uncertainty in the $K^\pm$ identification efficiency;
3. treatment of residual BE correlations;
4. overall normalization of reflections;
5. choice of the background parametrization, bin size of the mass spectra and mass range used in the fit;
6. variation in absolute value of the factor $\langle R\rangle$.

However, the systematic uncertainties arising from these effects affected mostly the overall normalization of the vector meson cross-sections, rather than the shapes of their angular distributions. Consequently, their influence on the values of the spin density matrix elements was found to be small compared with the statistical errors. The systematic error on ρ_{00} and the off-diagonal matrix elements for all three mesons in all x_p intervals arising from these uncertainties was conservatively taken to be ± 0.01.

The relative contributions of the reflections in different angular intervals were taken from JETSET, where isotropic angular distributions for the decay products of the vector mesons are assumed. This may result in additional systematic uncertainties of the ρ_{00} values for the ρ^0 and $\mathrm{K}^{*0}(892)$, for which the reflections from the vector mesons are important. These uncertainties were estimated by modifying the angular distributions of the reflections from the vector mesons, which were taken to have the form (11) with $\rho_{00} = 0.5$, close to the experimentally found values. The determination of the spin density matrix was then repeated, and the resulting elements of ρ_{00} were found to differ by less than 0.03 from those listed in Table 1, independent of the x_p range; this was assigned as the additional systematic error for the ρ^0 and $\mathrm{K}^{*0}(892)$.

For the ϕ, where the influence of reflections is negligible, the above systematic error was ignored. However, in this case one cannot exclude some distortion of the $\cos\theta_h$ distribution, especially for ϕ of large momentum, due to the small opening angle between the K^+ and K^- in the xy plane in the laboratory frame. This was estimated by comparing the $\cos\theta_h$ distributions in two different intervals of the azimuthal angle φ, which is closely correlated with the opening angle between the K^+ and K^- in the xy plane in the laboratory frame. From the values of ρ_{00} and $\mathrm{Re}\rho_{1-1}$ determined in the two φ intervals $\varphi/\pi = 0.25-0.75$ and $\varphi/\pi \neq 0.25-0.75$ and their comparison with the values determined in the full φ interval, no evidence for possible systematic biases in the ρ_{00} and $\mathrm{Re}\rho_{1-1}$ was seen within the statistical errors. The corresponding systematic errors on ρ_{00} and on the off-diagonal matrix elements for the ϕ were conservatively taken to be ± 0.03 and ± 0.02, respectively, in all x_p intervals.

A part of the observed spin alignment may arise from charmed particle decays into the vector and pseudoscalar mesons, since in this case the angular distribution of the vector meson decay products in the vector meson rest frame follows a $\cos^2\theta_h$ distribution with respect to the charmed particle direction. The effect was evaluated using the Monte Carlo simulation with measured charmed particle production rates taken from [26]. Its contribution to the measured ρ_{00} values was found to be negligible for $x_p \leq 0.3$ and less than 0.01 for $x_p \geq 0.3$, 0.4 and 0.5.

3.3 Discussion

Simple statistical models (see [4] and references therein) which might be applicable in the region of small x_p, assume that in the fragmentation process extra quark pairs are produced with both helicities of quarks being equally likely. If the helicities of the primary quark and secondary antiquark line up, a vector meson is produced. If the quark helicities are antiparallel, either a pseudoscalar meson is produced with a probability f or a vector meson with a probability $1-f$. Then $\rho_{00} = (1-f)/(2-f)$, with $0 \leq \rho_{00} \leq 0.5$. In terms of the ratio of pseudoscalar to vector meson production, P/V, such models [4] give $\rho_{00} = \frac{1}{2}(1-P/V)$. With the ρ_{00} values (13) and (14) close to 1/3, one has $P/V = 1/3$ as expected from spin counting. This agrees with the recent conclusions made from the analysis of particle production rates at LEP in [27–29], but not with the default value of the parameter $P/V = 1$ in the commonly used Monte Carlo models.

In the region of large x_p, it is interesting to compare the spin alignment of the vector mesons produced in the fragmentation of the primary quarks in $e^+e^- \to q\bar{q}$ and of the valence quarks of the incident mesons in meson-induced hadronic reactions. The latter was measured in the so-called transversity frame in the reactions $\pi^+ p \to \rho^0 + X$ and

$K^+p \to K^{*0}(892)+X$ at incident momentum of 250 GeV/c by the EHS-NA22 experiment [30]. In the transversity frame, $\cos\theta$ was defined as $\cos\theta = \vec{N}\cdot\vec{n}(\pi^-)$, with $\vec{N}$ being the unit vector normal to the reaction plane, and $\vec{n}(\pi^-)$ being a unit vector along the momentum of the π^- from the ρ^0 or $K^{*0}(892)$ decay in the resonance rest frame. In the Feynman variable range $x(\rho^0, K^{*0}) \geq 0.7$ ($x = 2p_L/\sqrt{s}$ where p_L is the longitudinal momentum in the centre of mass frame), the reported values are $\rho_{00}(\rho^0) = 0.10 \pm 0.04$ and $\rho_{00}(K^{*0}) = 0.13 \pm 0.04$. Small values of ρ_{00} in the transversity frame correspond to large values of ρ_{00} in the helicity frame. Thus the spin alignment of the vector mesons produced in e^+e^- collisions and in meson-induced reactions in the fragmentation regions appears to be qualitatively similar.

Several models give predictions on the values of ρ_{00} in the helicity frame for the vector mesons produced in the fragmentation region. The QCD-inspired model [6] is based on a picture where hadron production proceeds via independent soft gluon emission creating a $q\bar{q}$ pair. At each step of the chain, as the primary quark (or antiquark) remains highly energetic and undeflected, the vector coupling to the gluon conserves the quark helicity. At the end of the chain the primary quark catches a soft antiquark and forms the leading hadron. The vector mesons produced by such a mechanism are expected to be preferentially in the helicity $\lambda = \pm 1$ state with $\rho_{00} \approx 0$. In this picture the coupling of the hadronic wave function to nearly real quarks with very large rapidity difference was considered. This kinematical configuration, as noticed in [6], is different from that considered in other models [7–9] based on perturbative QCD, where the final hadron is made of quarks sharing the hadron energy equally. These models, contrary to the previous one, predict the dominance of the helicity $\lambda = 0$ state, with $\rho_{00} \approx 1$. A similar prediction was made in the model considered in [4]. The DELPHI results indicating that $\rho_{00} > 1/3$ for the vector mesons in the forward x_p region appear to be in better agreement with the models [4,7–9] predicting the preference of the helicity zero state.

The off-diagonal elements ρ_{1-1} of the spin density matrix for the ρ^0, K^{*0}(892) and ϕ (Table 1) were found to be consistent with zero in the x_p regions considered . Generally the off-diagonal elements are expected to be very small. However, according to [10–12], this may not be the case for the vector mesons due to coherence phenomena. Within present errors, no evidence is seen for such effects. In particular, this disagrees with the quantitative predictions of the ρ_{1-1} for the ρ^0, K^{*0}(892) and ϕ in hadronic Z^0 decays recently obtained in [12].

4 Summary

For the K^{*0}(892) and ϕ produced in the small x_p regions $0.1 \leq x_p \leq 0.3$ and $0.05 \leq x_p \leq 0.3$, respectively, the ρ_{00} spin density matrix element was measured to be: $\rho_{00}(K^{*0}) = 0.33 \pm 0.05$ and $\rho_{00}(\phi) = 0.30 \pm 0.04$ in the helicity frame. These results are consistent with no spin alignment and with the ratio of pseudoscalar to vector meson production $P/V = 1/3$ as expected from spin counting.

In the high x_p region, the K^{*0}(892) and ρ^0 appear to be produced with unequal populations in the three helicity states. Thus for $x_p \geq 0.4$, the ρ_{00} spin density matrix element was measured to be $\rho_{00}(K^{*0}) = 0.46 \pm 0.08$ and $\rho_{00}(\rho^0) = 0.43 \pm 0.05$, indicating that the helicity zero state is preferentially occupied. This agrees with the preference for the helicity zero states for the K^{*0}(892) and ρ^0 produced in the beam fragmentation region in hadronic K^+p and π^+p reactions , respectively.

For the ϕ in the same $x_p \geq 0.4$ region, no spin alignment was observed with $\rho_{00} = 0.30 \pm 0.04$. However in the high x_p region $x_p \geq 0.7$, $\rho_{00}(\phi) = 0.55 \pm 0.10$ for the ϕ in agreement with the value of $\rho_{00} = 0.54 \pm 0.08$ recently measured in the same $x_p \geq 0.7$ range by OPAL.

The off-diagonal elements ρ_{1-1} of the spin density matrix for the ρ^0, $\mathrm{K}^{*0}(892)$ and ϕ were found to be consistent with zero.

The measurements presented here, together with the OPAL results on the ϕ and $\mathrm{D}^{*\pm}$, show some evidence for spin alignment of the vector mesons produced in the fragmentation region, and thus contribute to an understanding of the role of spin in the hadronization process.

Acknowledgements

We are greatly indebted to our technical collaborators and to the funding agencies for their support in building and operating the DELPHI detector, and to the members of the CERN-SL Division for the excellent performance of the LEP collider.

References

[1] A. Blondel et al., in *Physics at LEP2*, CERN Yellow Preprint 96-01, Eds. G. Altarelli, T. Sjöstrand and F. Zwirner, Vol. 2, p. 103 (1996).
[2] B. Andersson, G. Gustafson, G. Ingelman and T. Sjöstrand, Phys. Rep. **97** (1983) 31.
[3] G. Marchesini and B.R. Webber, Nucl. Phys. **B238** (1984) 1.
[4] J.F. Donoghue, Phys. Rev. **D19** (1979) 2806.
[5] J.F. Nieves, Phys. Rev. **D20** (1979) 2775.
[6] J.E. Augustin and F.M. Renard, Nucl. Phys. **B162** (1980) 341.
[7] G.R. Farrar and D.R. Jackson, Phys. Rev. Lett. **35** (1975) 1416.
[8] A.I. Vainstein and V.I. Zakharov, Phys. Lett. **B72** (1978) 368.
[9] R. Suaya and J.S. Townsen, SLAC-PUB (1978) 2190.
[10] M. Anselmino, P. Kroll and B. Pire, Z. Phys. **C29** (1985) 135.
[11] A. Anselm, M. Anselmino, F. Murgia and M.G. Ryskin, hep-ph/9310234, published in J. Exp. Th. Phys. Lett. **60** (1994) 496.
[12] M. Anselmino, M. Bertini, F. Murgia and P. Quintairos, hep-ph/9704420, Torino Univ. Preprint DFTT 25/97, INFNCA-TH9707 (1997).
[13] HRS Collab., S. Abachi et al., Phys. Lett. **B199** (1987) 585.
[14] TPC Collab., H. Aihara et al., Phys. Rev. **D43** (1991) 29.
[15] CLEO Collab., Y. Kubota et al., Phys. Rev. **D44** (1991) 593.
[16] DELPHI Collab., P. Abreu et al., Z. Phys. **C68** (1995) 353.
[17] ALEPH Collab., D. Buskulic et al., Z. Phys. **C69** (1995) 393.
[18] OPAL Collab., K. Ackerstaff et al., CERN-PPE/96-192, submitted to Z. Phys. **C** and CERN-PPE/97-05, submitted to Z. Phys. **C**.
[19] DELPHI Collab., P. Abreu et al., Z. Phys. **C65** (1995) 587.
[20] DELPHI Collab., P. Abreu et al., Z. Phys. **C73** (1996) 61.
[21] DELPHI Collab., P. Aarnio et al., Nucl. Instr. Meth. **A303** (1991) 233.
[22] DELPHI Collab., P. Abreu et al., Nucl. Instr. Meth. **A378** (1996) 57.
[23] T. Sjöstrand, Comp. Phys. Comm. **82** (1994) 74; CERN Preprint CERN-TH. 7112/93 (1993, revised August 1994).
[24] DELPHI Collab., P. Abreu et al., Z. Phys. **C73** (1996) 11.
[25] DELPHI Collab., P. Abreu et al., Phys. Lett. **B361** (1995) 207.
[26] Particle Data Group, R.M. Barnett et al., Phys. Rev. **D54** (1996) 1.
[27] P.V. Chliapnikov and V.A. Uvarov, Phys. Lett. **B345** (1995) 313.
[28] F. Becattini, Z. Phys. **C69** (1996) 485.
[29] Yi-Jin Pei, Z. Phys. **C72** (1996) 39.
[30] EHS-NA22 Collab., N.M. Agababyan et al., Z. Phys. **C46** (1990) 387.

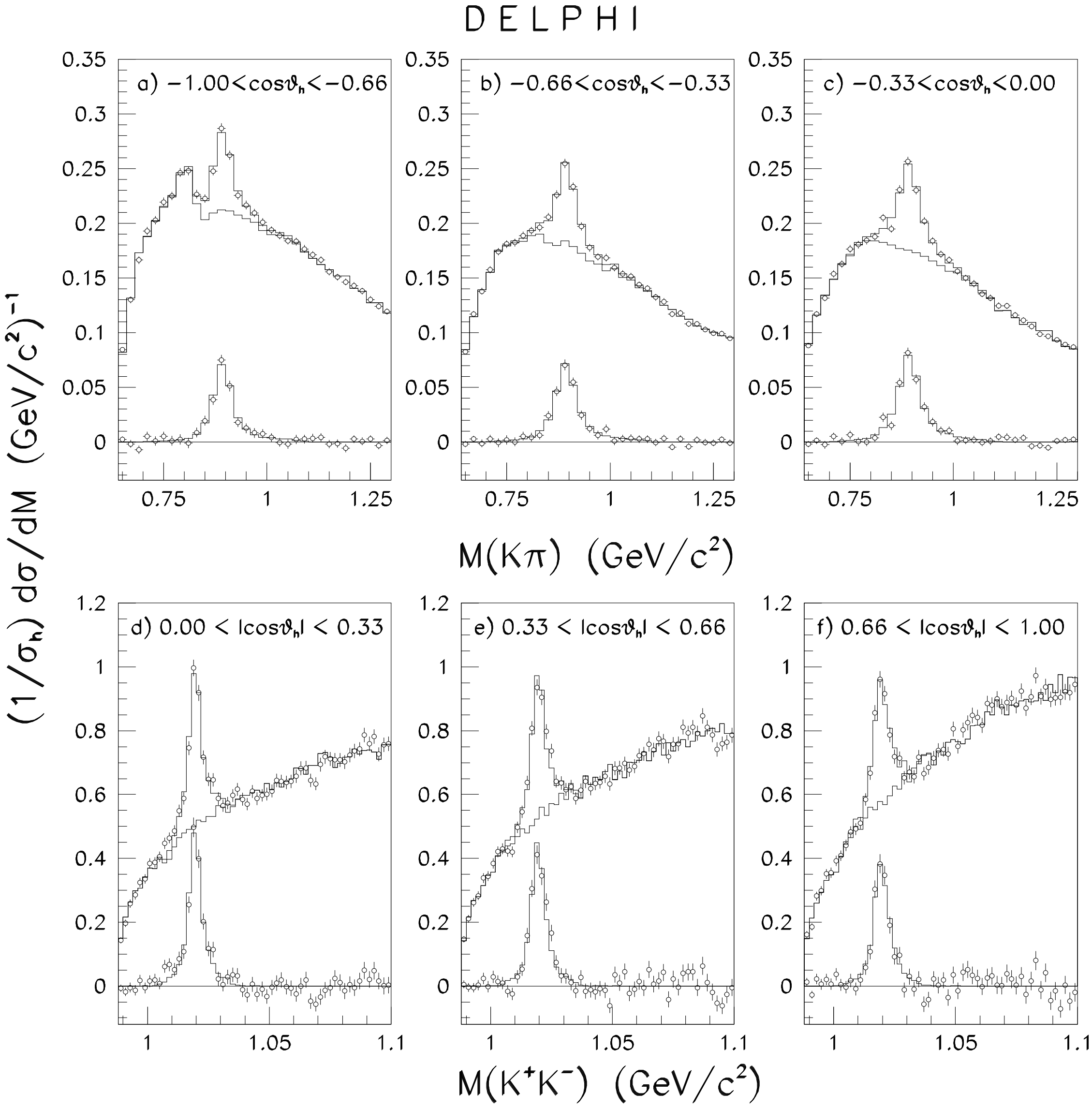

Figure 1: The invariant mass spectra of **(a-c)** $K^{\pm}\pi^{\mp}$ for $0.1 \leq x_p \leq 0.3$ and **(d-f)** K^+K^- for $0.05 \leq x_p \leq 0.3$ in the indicated $\cos\theta_h$ and $|\cos\theta_h|$ intervals for the uncorrected data (*open points*). The *upper histograms* are the results of the fit. The sum of the background and reflection function contributions is shown by the *lower histograms*. The *lower parts of the figures* present the data and the results of the fit after subtracting the background and reflection contributions.

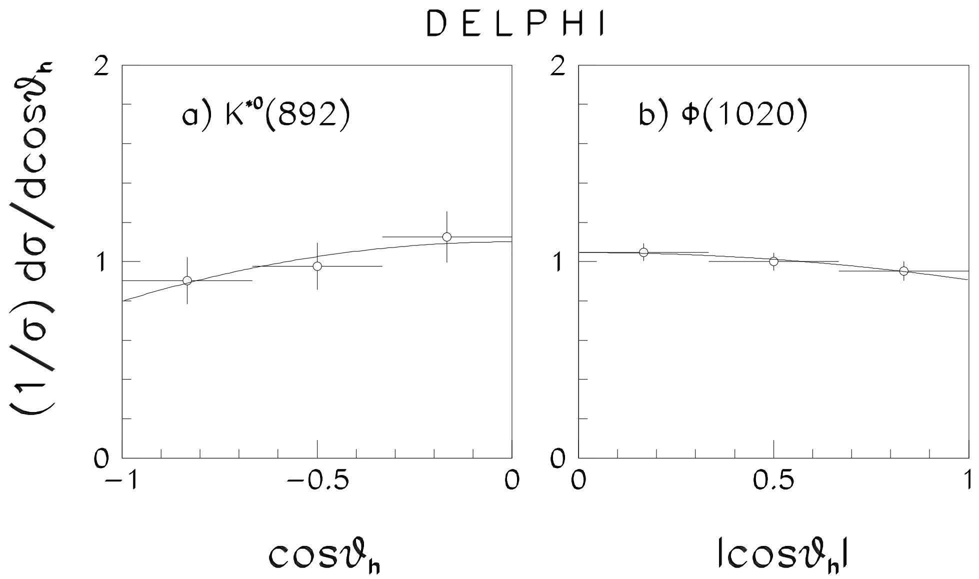

Figure 2: The $\cos\theta_h$ and $|\cos\theta_h|$ distributions of **a)** $K^{*0}(892)$ for $0.1 \leq x_p \leq 0.3$ and **b)** ϕ for $0.05 \leq x_p \leq 0.3$. The *curves* are the results of the fit to the function (11).

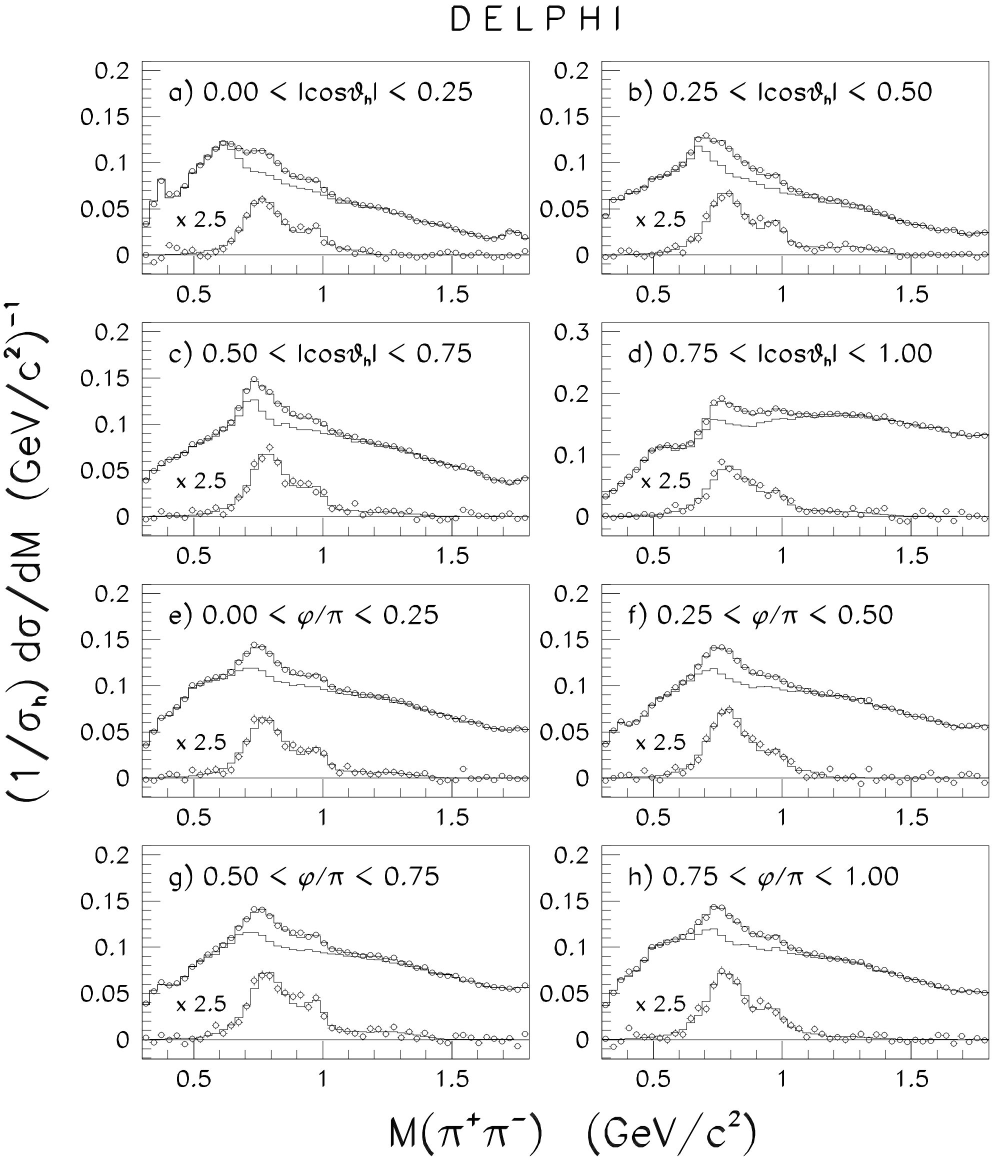

Figure 3: The $\pi^+\pi^-$ invariant mass spectra for the $x_p \geq 0.4$ range in the indicated $|\cos\theta_h|$ **(a-d)** and φ **(e-h)** intervals for the uncorrected data (*open points*). The *upper histograms* are the results of the fit. The sum of the background and reflection function contributions is shown by the *lower histograms*. The *lower parts of the figures* present the data and the results of the fit for the ρ^0, $f_0(980)$ and $f_2(1270)$ contributions after subtracting the background and reflections.

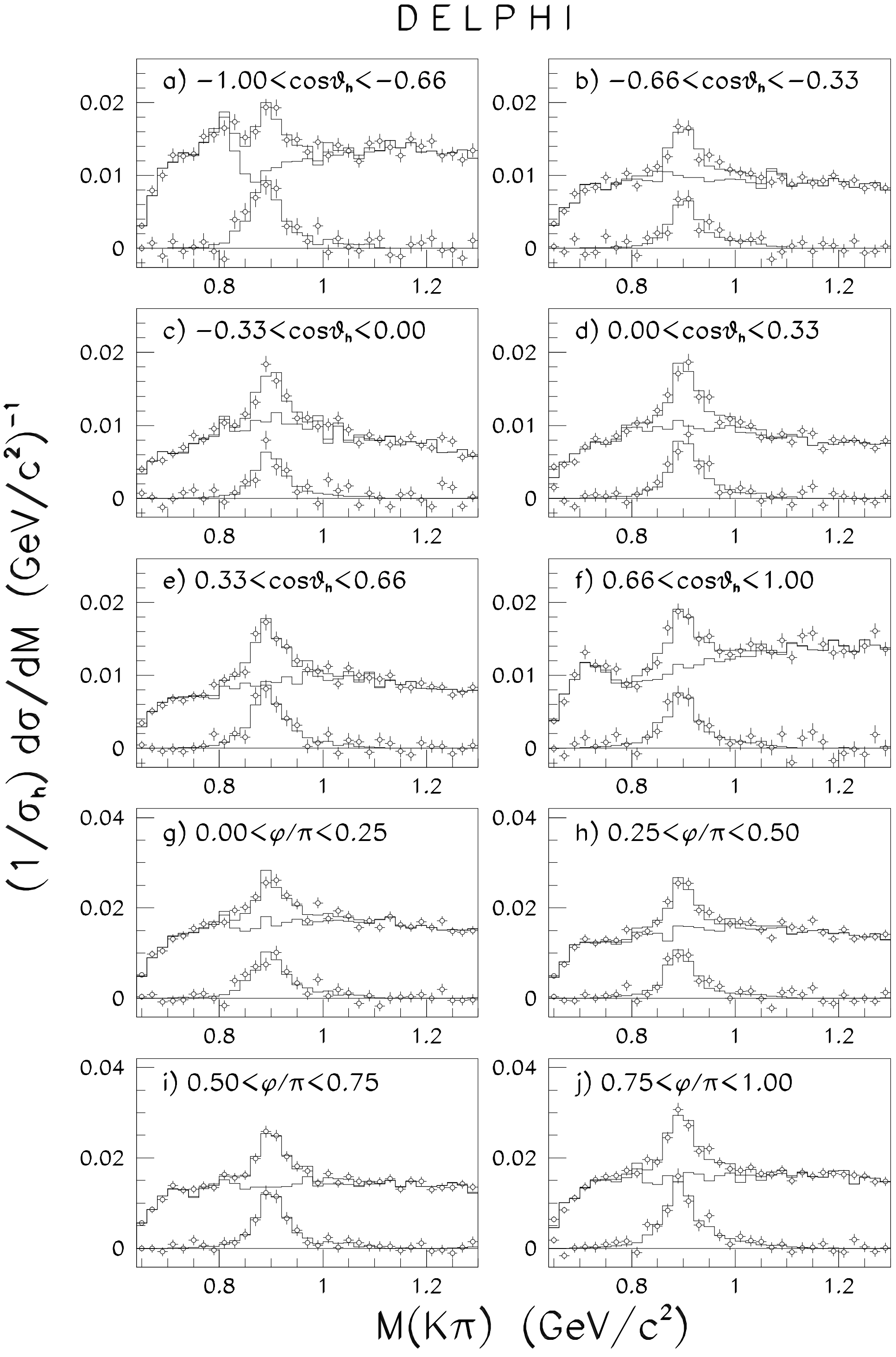

Figure 4: The $K^{\pm}\pi^{\mp}$ invariant mass spectra for the $x_p \geq 0.4$ range in the indicated $\cos\theta_h$ **(a-f)** and φ **(g-j)** intervals for the uncorrected data (*open points*). The *upper histograms* are the results of the fit. The sum of the background and reflection function contributions is shown by the *lower histograms*. The *lower parts of the figures* present the data and the results of the fit after subtracting the background and reflection contributions.

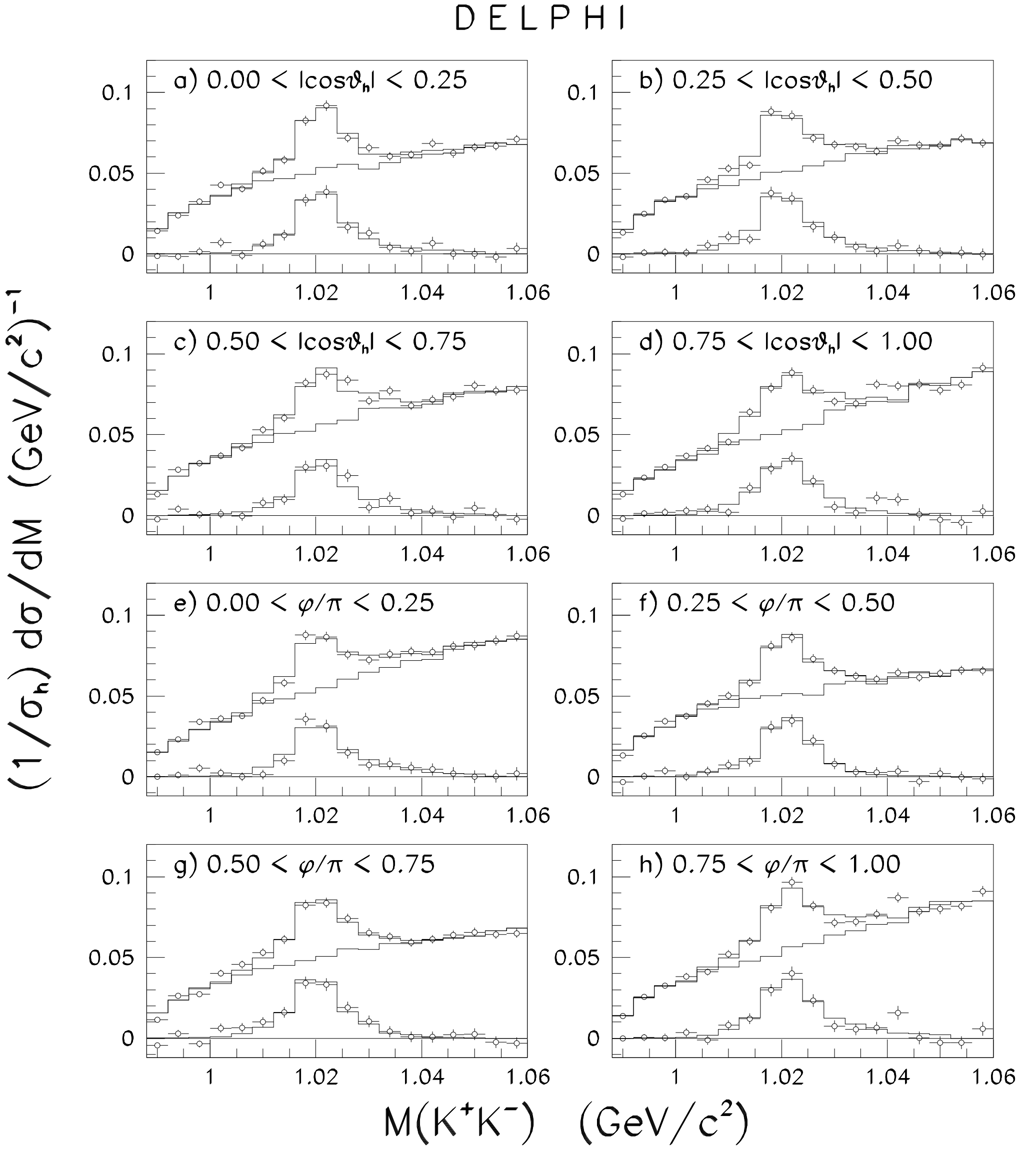

Figure 5: The K^+K^- invariant mass spectra for the $x_p \geq 0.4$ range in the indicated $|\cos\theta_h|$ **(a-d)** and φ **(e-h)** intervals for the uncorrected data (*open points*). The *upper histograms* are the results of the fit. The sum of the background and reflection function contributions is shown by the *lower histograms*. The *lower parts of the figures* present the data and the results of the fit after subtracting the background and reflection contributions.

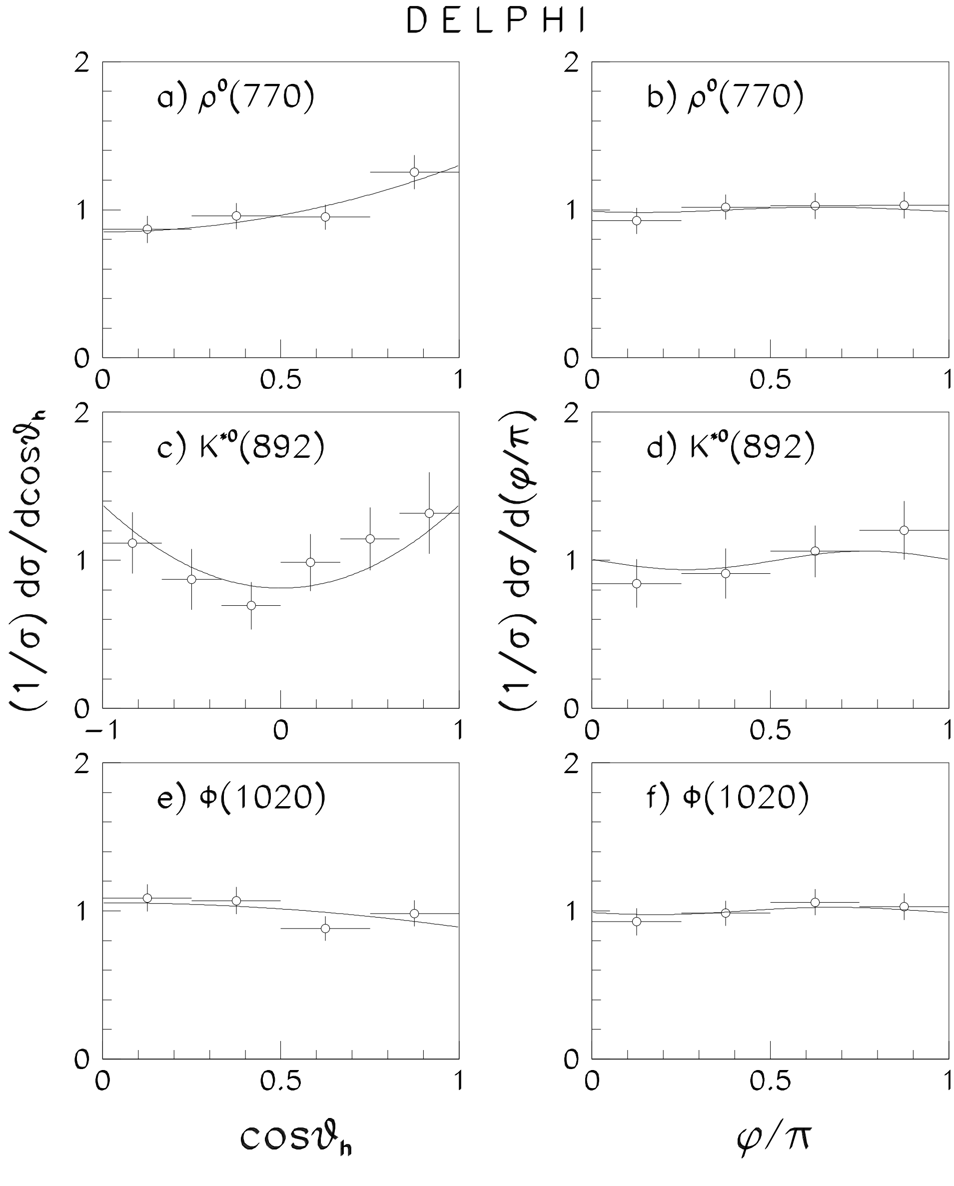

Figure 6: The $\cos\theta_h$ and φ distributions of **(a, b)** the ρ^0, **(c, d)** the $K^{*0}(892)$, and **(e, f)** the ϕ for the $x_p \geq 0.4$ range. The *curves* are the results of the fit to the functions (11) (a, c, e) and (12) (b, d, f).